International Journal on Artificial Intelligence Tools
Vol. 28, No. 1 (2019) 1950005 (21 pages)
© World Scientific Publishing Company
DOI: 10.1142/S0218213019500052

Int. J. Artif. Intell. Tools 2019.28. Downloaded from www.worldscientific.com
by 14.145.175.103 on 03/18/20. Re-use and distribution is strictly not permitted, except for Open Access articles.

Artificial Immune System with Negative Selection Applied to Facial Biometry Based on Binary Pattern Characteristics

Jadiel C. Silva*,‡, Fernando P. A. Lima*,§, Anna Diva P. Lotufo*,¶
and Jorge M. M. C. P. Batista†

*Department of Electrical Engineering, Intelligent Systems Laboratory – SINTEL
São Paulo State University – UNESP, Av. Brasil, 56 – Ilha Solteira
Campus de Ilha Solteira, 15385-000, São Paulo, SP, Brasil
†Department of Electrical and Computer Engineering, Institute of Systems and Robotics
University of Coimbra, Portugal, Pinhal de Marrocos, Polo II – Coimbra
‡jadiel@mail.uft.edu.br
§engfernandoparra@gmail.com
¶anna.lotufo@ unesp.br
†btista@isr.uc.pt

Received 12 November 2017
Accepted 11 February 2019
Published 28 February 2019

This work aims to explore resources and alternatives for 3D facial biometry using Binary Patterns. A 3D facial geometry image is converted into two 2D representations, appointed as descriptors: A Depth Map and an Azimuthal Projection Distance Image. The first is known as traditional facial geometry, and the second is normal facial geometry that is able to capture the information of different geometries. The characteristics of Local Binary Patterns, Local Phase Quantisers and Gabor Binary Patterns were used with the Depth Map and Azimuthal Projection Distance Image to produce six new facial descriptors: 3D Local Binary Patterns, Local Azimuthal Binary Patterns, Local Depth Phase Quantisers, Local Azimuthal Phase Patterns, and Local Depth Gabor Binary Pattern Magnitudes and Phases. Then, this work uses the immune concept to propose a new approach to realize facial biometry, where the eight new facial descriptors were applied to an Artificial Intelligence algorithm named Artificial Immune Systems of Negative Selection. The analysis of the results shows the efficiency, robustness, precision and reliability of this approach, encouraging further research in this area.

Keywords: Identity recognition; binary pattern; facial geometry; detection and classification; artificial intelligence; artificial immune system of negative selection; intelligent systems.

1. Introduction

Recent research efforts have focused on recognizing complex and spontaneous emotional phenomena. This is due to the limited available datasets of expressions that contain only affective faces: angry, contempt, disgust, fear, happiness, sadness and surprise.[1]

Some conditions such as make-up, beards, illumination and occlusion make the facial expression recognition system highly sensitive. Additionally, when using 2D facial images, it is necessary to maintain a consistent facial pose (preferentially frontal)

Int. J. Artif. Intell. Tools 2019.28. Downloaded from www.worldscientific.com
by 14.145.175.103 on 03/18/20. Re-use and distribution is strictly not permitted, except for Open Access articles.

to obtain good recognition performance. Therefore, several 2D views must be used to guarantee full capture of the facial information.[2]

The subarea of Identity Recognition (IR) is inside the field of computational intelligence. Its use is as an alternative to the identification and authentication aspects of traditional methods, such as the use of keys, identification cards and passwords. Facial recognition technology is applied in PC access, airport criminal identification vigilance, ATM (Automatic Teller Machine) transactions, *etc*.

A relatively new area of IR research are the 3D facial geometry data, which allows for a greater amount of information to be captured, including outside the 2D plane, removing the problems of lighting and representations inherent in 2D data. 3D data have been employed for the complete recognition of facial expression[2] and facial detection of Action Unit (AU).[3] So far, most of the investigations of facial features performed in 3D static meshes are employed on the basis of facial spots,[4–6] on screen blemishes,[7,8] or in Morphable models[9,10] and, in the 2D representations, as the map and curvature of the depth images were explored.[11]

The technique of Local Binary Patterns (LBPs)[12] has been extensively applied to the problems of facial expression recognition[13] and IR.[14] They are a useful resource type because they are simple and fast to encode the image of each pixel by the binary numbers that reflect the local neighborhood. Variants of the LBPs technique have been proposed to improve performance of the basic feature, such as: Local Phase Quantisers (LPQ)[15] and Gabor Binary Patterns (GBPs).[16]

The principal work found in the literature was conducted by Sandbach *et al*.,[2] where the authors propose various methods based on the application of binary patterns to the recognition of an action units AU. The recognition system used the algorithm Gentle Boost on the Bosphorus database of facial images and obtained promising results. For example, for the 3D Local Binary Pattern (3DLBP) descriptor, the mean is approximately 95.6% assurance. Savran *et al*.[17] presented an innovative 3D facial expression image analysis, since so far, most studies were conducted with 2D images that contain data limitations, while in 3D images possible to capture facial surface data, as well as being less disturbed by illumination and pose (preferentially frontal). The comparative results of tests with 2D and 3D images are presented and it is observed that 3D images work best with 96.1% correct detection. Another approach presented by Matuszewski *et al.*[18] describes the importance of facial expression and facial recognition for different expressions. The database used is 4D (Hi4D-ADSIP), and the tests provide an average of 83% assurance. This database is promising due to the creation of an extension with representative face images from patients with stroke, Bell paralysis and Parkinson's disease.

Encouraging results were introduced by Silva *et al.*,[19] and presented tests and results obtained for the proposed methodology were applied to IR based on AIS. The main objective was to evaluate which is the best expression to realize IR and validate the performance of the new solution of the IR because IR based on faces is one of the most important biometric characteristics applied in several areas, and this importance is increasing, as is research in intelligence systems. The proposal presented excellent results

Int. J. Artif. Intell. Tools 2019.28. Downloaded from www.worldscientific.com
by 14.145.175.103 on 03/18/20. Re-use and distribution is strictly not permitted, except for Open Access articles.

with a mean index of 99.01% of correct classification. This concludes that the system is efficient and robust, stimulating the continuation and development of this research. Thus, with a need for efficiency, robustness, precision and reliability, this present work is based on the methodology introduced by Silva *et al.*,[19] where the immune concept is used to propose this new approach to realizing IR, evaluating the best descriptor, the best expressions to accomplish IR and validation of the performance of the new approach based on the AIS.

Selection and classification feature methods used for 3D facial expression analysis are generally similar to those used for 2D cases. A wide variety of classification techniques have been employed in 3D facial expression recognition systems. These include methods such as discriminant analysis,[5,21,21] linear classifiers,[22] nearest neighborhood rating,[23] grouping,[24] probability and maximum classifiers.[25–30] More recently the use of Artificial Intelligence (AI) has taken enormous proportions in the classifier studies and several other areas, such as Artificial Neural Networks (ANN).[31–33] However, the present work will use a new proposal with, the Artificial Immune System (AIS) which has some advantages when compared to Neural Networks.

Firstly, other methods of exploring 3D facial geometry information have been explored through the use of binary pattern methods where 3D facial geometry is converted into two 2D representations: A Depth Map (DM)[3] and an Azimuthal Projection Distance Image (APDI).[2] Posteriorly, the binary approach, which is widely applied to IR problems,[14] is explored for 3D facial expressions, termed LBP.[12] This technique is useful because it is simple and quick to codify the image by pixels with binary numbers that represent the local neighborhood. Variants of the LBP have also been used to improve on the performance of the basic feature: LPQs[15] and GBPs.[16] These descriptors were chosen and developed because they are the ones with the greatest impact factor in the pattern recognition literature.

Finally, to perform the facial biometry, an AI namely AIS was used, based on the Negative Selection Algorithm (NSA). AIS is a promising strategy based on the Biological Immune System (BIS) that computationally reproduces the main characteristics and abilities of the BIS.[31] Initially, AIS was proposed to solve computational security problems, and it presented satisfactory and efficient results.[31] Afterwards, De Castro and Timmis[32] showed that AIS is an excellent tool for performing image recognition due to the natural characteristics of pattern recognition and continuous learning, and it is able to include new images in the diagnosis process without the need to reset the memory of the system. The algorithm is executed in two phases: Censor and Monitoring. The Censor phase defines the set of proper chains (S) for which protection is desired, generating random chains and evaluating the affinity (*match*) with each one, and in the Monitoring phase is when the affinity of the chains and the detectors generated in the Censor phase is evaluated.

This paper is organized as follows. Section 2 presents the methodology used and Section 3 describes the artificial immune system (AIS). Section 4 shows the identity recognition. The facial geometry representation is presented in Section 5, as well as the

LBP, LPQ and GBP. The tests and results are in Sections 6 and 7, respectively. Finally, Section 8 presents the conclusion and suggestions for future work.

2. Methodology

Firstly, the 3D facial geometry is converted into two 2D representations (DM and APDI), and then an algorithm is implemented to allow for exploration of new types of resources to analyze facial expressions. Secondly, the DM and APDI facial geometries were used in conjunction with the LBP features to produce two new image descriptors: 3DLBP and Local Azimuthal Binary Patterns (LABP), respectively.[2]

Figure 1 shows the system in which the DM and APDI are 2D images that represent the 3D facial geometry. These images are computed to obtain the LBP, which leads to the 3DLBP and LABP.

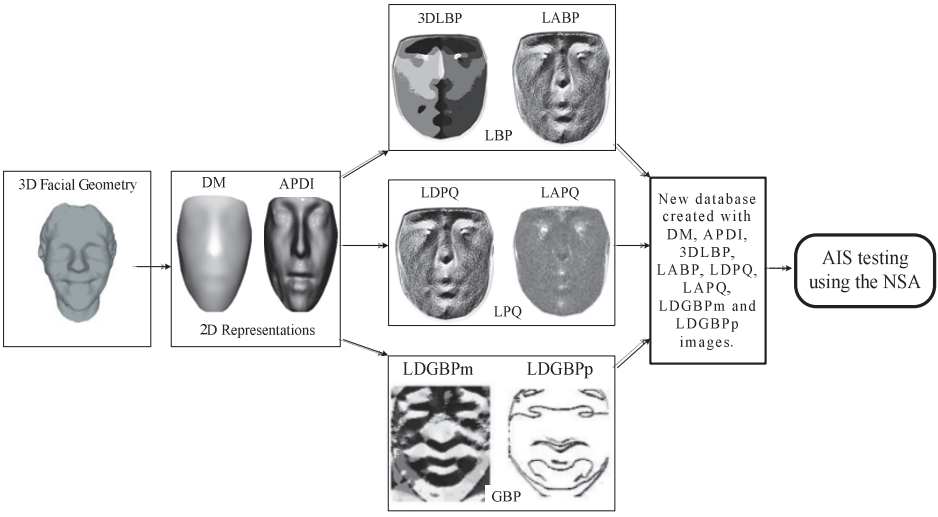

Fig. 1. Proposed system.

This same methodology was implemented using LPQ. Then, two new image descriptors were produced from the DM and APDI facial geometries: Local Depth Phase Quantisers (LDPQ) and Local Azimuthal Phase Quantisers (LAPQ), respectively. Posteriorly, the DM facial geometries were used with the characteristic GBP in which the magnitude and phase of these are taken as new images, giving rise to two other new descriptors: Local Depth Gabor Binary Patterns Magnitude (LDGBPm) and the Local Depth Gabor Binary Patterns Phase (LDGBPp).

Thus, from the image database[37] a new database is created with DM, APDI, 3DLBP, LABP, LDPQ, LAPQ, LDGBPm and LDGBPp images.

Then, these images were submitted separately to AIS tests using the NSA as proposed by Forrest *et al*.[33] The dataset can be used for either censor or monitoring, and a maximum limit of 30% of the data is needed to generate the detector set. This limit is imposed

Int. J. Artif. Intell. Tools 2019.28. Downloaded from www.worldscientific.com
by 14.145.175.103 on 03/18/20. Re-use and distribution is strictly not permitted, except for Open Access articles.

Int. J. Artif. Intell. Tools 2019.28. Downloaded from www.worldscientific.com
by 14.145.175.103 on 03/18/20. Re-use and distribution is strictly not permitted, except for Open Access articles.

according to the BIS, where the quantity of detectors existing in the living body is approximately 30% of the infecting agents present. Therefore, a maximum of 30% of the data is adopted for use as detectors in the censor phase, making the procedure dynamic and real.

To evaluate the performance of the method, tests were done separately for each of the eight image representations. The purpose of these tests was to evaluate the best descriptor, the best expression to perform the IR and to validate the performance of the new IR solution based on AIS.

3. Artificial Immune System (AIS)

In recent years, researchers have started new studies in the field of natural phenomena, especially those related to natural or biological systems, which efficiently solve problems in various regions of the human body, going beyond any technological strategy.[32] Among the several phenomena studied, can be mention some examples of natural systems used in recent years, which have been very successful in the development of technological strategies applied to the solution of highly complex problems: Genetic algorithms, evolutionary algorithms, computation by DNA or molecular, behavior of insect colonies, artificial neural networks and the immune system.[32]

3.1. *Negative selection algorithm* (*NSA*)

The NSA proposed by Forrest *et al.*[33] to detect changes in systems based on the negative selection of *T* lymphocytes, being a technique that is based on the process of pattern recognition exercised by the BIS, elaborated as a computational model. Therefore, this is the process that represents the discrimination that the organism makes with the cells, between proper and non-proper. This algorithm works in two phases according to the following description:[32,34]

(1) **Censor Phase**

(a) first, a set of the desired proper chains (*S*) to protect are defined,

(b) then, random chains are generated, and the degree of matching and affinity between them and the proper chains are evaluated. If the affinity is above a predefined value, the chain is rejected. Otherwise, it is categorized as a detector in the detector set (*R*).

(2) **Monitoring Phase**

The affinity evaluation between each chain and the detector set is done by considering a set of desired chains to protect. Then, a non-proper element is identified when the affinity is above a predefined value.

Figure 2 presents the flowchart of the censor (a) and monitoring (b) of the NSA.

The advantage of using the AIS is that it does not have a training phase, such as that performed in the ANN, in addition to using a reduced set of information to perform the

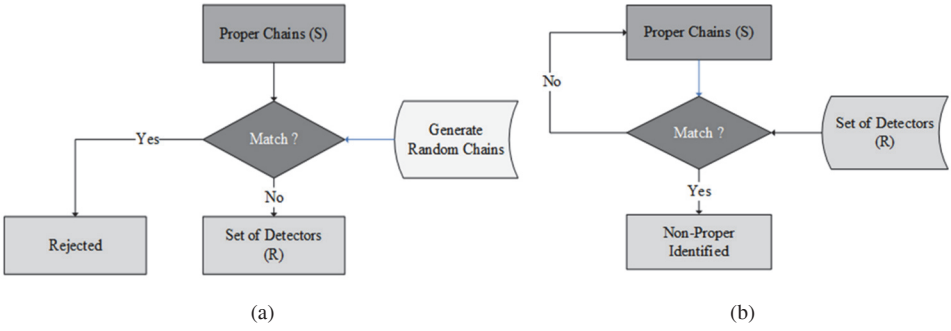

Fig. 2. Flowchart of the NSA. (a) Censor phase and (b) Monitoring phase.

classification (concept of distributed detection), generating a great reduction in the system's processing time.

3.2. *Matching and affinity criteria*

A criterion known as matching is used, and the results are classified as perfect or partial as follows:[35]

- Perfect – The two chains under analysis must be equal with the same values in every position.
- Partial – The two chains under analysis do not need to be equal, and only a number of positions within the pattern must have the same value to confirm the matching. This number is called the affinity rate (T_{af}), which was previously defined.

The T_{af} was proposed by Bradley[36] and is defined by:

$$T_{af} = \frac{An}{At} * 100 \tag{1}$$

where An is the quantity of normal chains in the problem (proper chains), and At is the quantity of chains in the problem (proper and non-proper chains).

For the IR system proposed in this work, the quantity of images analyzed was 520 ($At = 520$), and the quantity of images used to generate the proper detectors was 416 ($An = 416$). Therefore, the T_{af} is 80%, i.e., to confirm that matching exists between the two patterns, it is necessary that a minimum of 80% of the points be equal/match, then the correspondence strategy is partial.

4. Identity Recognition (IR)

Interest in facial biometric studies has been increasingly fast-paced, mainly due to research associated with AI. With facial recognition, it is possible to build systems to identify and verify a person. Due to its natural interpretation (human visual identification based on facial analysis) and low intrusion (in contrast to digital impressions), facial recognition is one of the most important biometric characteristics.[15]

Int. J. Artif. Intell. Tools 2019.28. Downloaded from www.worldscientific.com
by 14.145.175.103 on 03/18/20. Re-use and distribution is strictly not permitted, except for Open Access articles.

Int. J. Artif. Intell. Tools 2019.28. Downloaded from www.worldscientific.com
by 14.145.175.103 on 03/18/20. Re-use and distribution is strictly not permitted, except for Open Access articles.

A new area in IR research is 3D facial geometry, which allows for the capture of a great quantity of information. Therefore, 3D data are widely used for facial recognition.[2] Thus, the Institute of Systems and Robotics Laboratory (ISR) of Coimbra University developed a high-resolution 4D platform to build a database of eight different expressions from 65 people, for which seven participants repeated these expressions four times, resulting in 774 expressions and 38 700 3D models. In this database, only face dynamism and not head movement was considered. The tests in this paper used these images.[37]

Several research studies were developed using static facial images of each individual as a biometric (statistical analysis). However, facial dynamics are less affected by physical changes, such as aging, weight, the use of glasses, beards, *etc*., and research shows that this dynamic facial information can be successfully used to identify age, sex and IR. Furthermore, texture analysis is an important area in artificial and computational vision because most surfaces contain unique textures, making it possible to interpret the use of an artificial vision system by varying the optical properties. Therefore, texture is an important source of information in facial classification.[15]

In this study, the texture is defined as the spatial variation of pixel intensity in an image and the functional relationship between these pixels and their neighbors. The methodology used to obtain images using the representation technique of facial geometry was presented in Section 2. Additionally, the binary pattern and use of AIS to realize facial recognition are discussed.

5. Facial Geometry Representation

The DM is created by defining a regular grid of x and y values and using Delaunay triangulation to interpolate the facial grid height, which originates a regular grid of z values constituting the DM,[38] and example of this image is shown in Fig. 4(a).

It is also possible to delineate a second representation, APDI.[2] The objective in computing the APDI is to find a representation that allows for an exact comparison of the normal directions and local neighborhood. The Azimuthal Equidistant Projection (AEP) is able to project perpendiculars from points in a Euclidian space according to the direction and is used to capture the local variations in facial form.[39] This representation can be applied to the perpendicular to project each direction of the 3D position onto a 2D Euclidian surface.

Therefore, for a regular grid of perpendiculars defined according to $n(i,j) = (u_{i,j}, v_{i,j}, w_{i,j})$, where each point of the AEP on the surface is given by $p(i,j) = (x_{i,j}, y_{i,j})$ and is defined according to[2]:

$$x_{i,j} = k' \cos\theta(i,j) \sin[\emptyset(i,j) - \hat{\emptyset}(i,j)] \tag{2}$$

$$y_{i,j} = k'\{\cos\hat{\theta}(i,j) \sin\emptyset(i,j) - \sin\hat{\emptyset}(i,j) \cos\theta(i,j) \cos[\emptyset(i,j) - \hat{\emptyset}(i,j)]\} \tag{3}$$

where $\theta(i,j) = \frac{\pi}{2} - \arcsin(w_{i,j})$ is the elevation angle measured from the z axis, $\emptyset(i,j) = \arctan\frac{v_{i,j}}{u_{i,j}}$ is the azimuth angle, $\hat{\theta}(i,j)$ and $\hat{\emptyset}(i,j)$ are the elevation and azimuth

of the perpendicular $\hat{n}(i,j)$ at point p, and $k' = \frac{c}{sin(c)}$, where c is defined as:

$$\cos(c) = \sin\hat{\theta}(i,j)\sin\emptyset(i,j) + \cos\hat{\emptyset}(i,j)\cos\theta(i,j)\cos\left[\emptyset(i,j) - \hat{\emptyset}(i,j)\right]. \quad (4)$$

The objective is to compare the projection of the neighboring points of coordinates, where $\hat{\theta}$ and $\hat{\emptyset}$ are defined by $\pi/2$ and 0, respectively, such that the distance calculated between the projection and reference perpendicular $\hat{n} = (1,0,0)$ creates an appropriate image for posterior analysis.

Using the identity $\cos(c) = \sin\theta(i,j)$, $x_{i,j}$, $y_{i,j}$ can be simplified to:

$$x_{i,j} = k'\cos\theta(i,j)\sin\emptyset(i,j). \quad (5)$$

$$y_{i,j} = k'\cos\theta(i,j)\cos\emptyset(i,j). \quad (6)$$

Based on this formulation, the distances between the perpendiculars on the Euclidean space can be found directly, and this simplification reduces the complexity of the extraction function. These coordinates are used to find an absolute distance from the origin defined by $d_{i,j} = \sqrt{x_{i,j}^2 + y_{i,j}^2}$ when employing the Binary Pattern descriptor. This originates the APDI, and example of this image is shown in Fig. 4(b).

5.1. *Local Binary Pattern* (*LBP*)

The LBP was initially used to analyze textures[12] and later used in recognition of facial images. This technique describes an image as a composition of micro-patterns and has been demonstrated successfully in the IR field.[14]

The methodology behind LBP involves attributing a binary value to each image pixel. This value is determined by computing a matrix containing the neighboring pixels, where each neighbor is compared to the central value. This is done by analyzing the difference between the gray-scale value of each pixel in the image and its neighbors. Thus, for each image *I*, a neighborhood is defined as a circle around each pixel with a radius *r* and *a* quantity of points spaced in *P* angles around the circumference. The central pixel is used as a reference to attribute binary bits to the pixels in the neighborhood, producing a binary number for each pixel according to the following equation[2]:

$$LBP_{(P,R)} = \sum_{p=0}^{P} 2^P s\big(I(xp,yp) - (xc,yc)\big) \quad (7)$$

where (*xc*, *yc*), (*xp*, *yp*) are the central pixel and the neighbors, respectively, and *P* is the quantity of neighbors.

Thus, the LBP obtains the values for each neighbor, concatenating and converting the values from a decimal base into a binary number, generated by substituting the central value for *v*. Figure 3 shows how this process is realized for the images in this work with an example of a 3 × 3 matrix of neighboring pixels.

Int. J. Artif. Intell. Tools 2019.28. Downloaded from www.worldscientific.com
by 14.145.175.103 on 03/18/20. Re-use and distribution is strictly not permitted, except for Open Access articles.

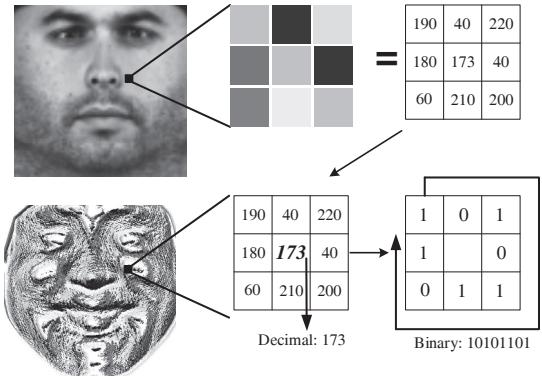

Fig. 3. Process realized by the LBP operator.

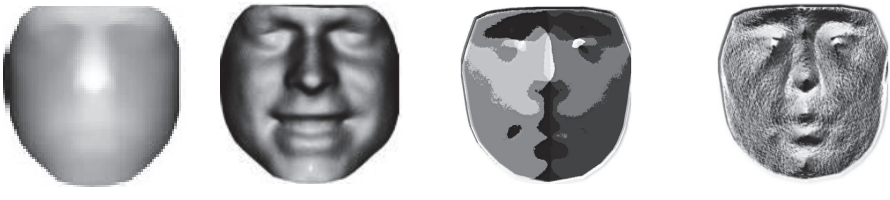

(a) (b) (c) (d)

Fig. 4. (a) DM, (b) APDI, (c) 3DLBP and (d) LABP for a subject in the database.[37]

Therefore, the LBP operator is able to codify structural facial information in 3D surfaces. Thus, the representation of the DM in 3D leads to the 3DLBP,[40] and the APDI representation gives rise to the LABP.[2] Examples of these images are shown in Figs. 4(c) and 4(d), respectively.[2]

5.2. *Local Phase Quantiser (LPQ)*

The LPQ method is based on the extraction of local phase information that contains important directional characteristics that describe facial deformations.[15] This property originates from the Fourier phase spectrum.[15] When performing digital imaging processing, the discrete model for spatially invariant undefination of an original image $f(x)$ results in an observed image $g(x)$. This image $g(x)$ can be expressed by convolution, as given by equation:[41]

$$g(x) = (f^{*}h)(x) \tag{8}$$

where $h(x)$ is the deflection point propagation function (PSF), * denotes 2D convolution, and x is a coordinate vector $[x, y]^T$.

Transforming this convolution into the Fourier domain yields:

$$G(u) = F(u)H(u) \tag{9}$$

Int. J. Artif. Intell. Tools 2019.28. Downloaded from www.worldscientific.com
by 14.145.175.103 on 03/18/20. Re-use and distribution is strictly not permitted, except for Open Access articles.

Int. J. Artif. Intell. Tools 2019.28. Downloaded from www.worldscientific.com
by 14.145.175.103 on 03/18/20. Re-use and distribution is strictly not permitted, except for Open Access articles.

where $G(u)$, $F(u)$ and $H(u)$ are the Discrete Fourier Transform (DFT) of the defocused image $g(x)$, the original image $f(x)$, and the PSF $h(x)$, respectively, and u is a coordinate vector $[u, v]^T$.

The Short-Term Fourier Transform (STFT)[2] is calculated on four different frequency pairs (Eq. (11)) to calculate eight binary digits for each pixel, which are then used for computational codes using the LBQ expression; alternately, local phase information can be extracted using 2D DFT, similar to LBP. For a point $f(x)$ with MxM pixels in the neighborhood of Nx, STFT is defined as:

$$F(u,x) = \sum_{y \in Nx} f(x-y)e^{-j2\pi u^T y} = w_u^T fx \tag{10}$$

where w_u^T is the base vector of 2D DFT at the frequency of u, and fx is another vector containing all M^2 of the Nx image samples.

Thus, STFT can be efficiently implemented from the above equation using the 2D convolutions of $f(x)*e^{-j2\pi u^T x}$ for all u. Then, four pairs of complex coefficients of the frequencies are employed:

$$u_1 = [a, 0]^T, \;\; u_2 = [0, a]^T, \;\; u_3 = [a, a]^T \;\text{ and }\; u_4 = [a, -a]^T \tag{11}$$

where a is scalar frequency below the first pass through zero in $H(u)$.[41]

Figure 5(a) shows the pixel input image in the neighborhood of Nx, and Fig. 5(b) shows by means of the white circles the four pairs of complex coefficients of the frequency employed.

Thus, the four pairs of complex coefficients of the frequencies indicated in Fig. 4(b) and their symmetrical counterparts are the $8Fx$ components in which most of the texture information in the neighborhood is concentrated.[42]

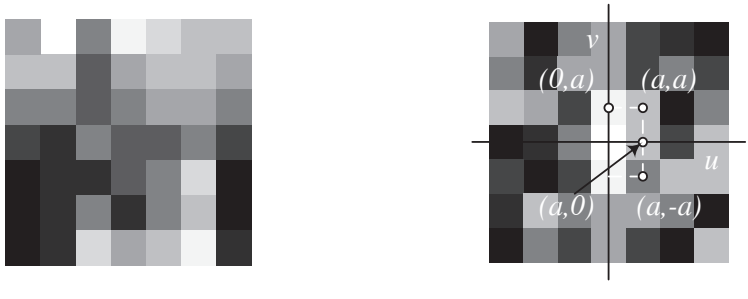

(a) (b)

Fig. 5. (a) Input image of neighboring pixels Nx and (b) Fourier transform module $|F_w\,(u)|$ of the input image.

The LPQ method was applied to DM and APDI, yielding two new descriptors: LDPQ and LAPQ. Examples are shown in Figs. 6(a) and 6(b), respectively.[2]

5.3. *Gabor Binary Patterns* (*GBP*)

Denis Gabor[43] proposed the Gabor transform, and over the years and with various studies of this technique, Gabor Filters have been widely used for the capture of structural

Int. J. Artif. Intell. Tools 2019.28. Downloaded from www.worldscientific.com
by 14.145.175.103 on 03/18/20. Re-use and distribution is strictly not permitted, except for Open Access articles.

information of images and in 2D facial expression recognition,[44] as well as 3D analysis.[17] With this method, it is possible to improve the facial characteristics, improving the robustness of the LBP when there are changes in lighting.[45]

As proposed by Sandbach *et al.*,[2] Gabor Filters can be used at four different scales and four orientations. Each of the descriptors is composed of a magnitude component and a phase component. The two-dimensional Gabor transform is a two-dimensional Gaussian function modulated with an oriented sinusoid containing a certain frequency W and orientation θ. The two-dimensional shape in the space and frequency domain can be expressed by the following equations, respectively:

$$g(x,y) = \left(\frac{1}{2\pi\sigma_x\sigma_y}\right)\exp\left[-\frac{1}{2}\left(\frac{x^2}{\sigma_x^2}+\frac{y^2}{\sigma_y^2}\right)+2\pi jWx\right]. \tag{12}$$

$$G(u,v) = \exp\left\{-\frac{1}{2}\left[\frac{(u-W)^2}{\sigma_u^2}+\frac{v^2}{\sigma_v^2}\right]\right\}. \tag{13}$$

It can be affirmed that the transfer function of the filters used consists of a radial Gabor filter multiplied by the angular Gaussian component, as follows:[2]

$$G(u)_{v,\theta} = \exp\left(\frac{-(\log(v|u|))^2}{2(\log\sigma)^2}\right)\exp\left(\frac{-(\angle u-\theta)^2}{2\sigma_\emptyset}\right) \tag{14}$$

where σ and $\sigma_\emptyset$ define the spread of the filter in the radial and angular directions, respectively, and v and θ are the scale and orientation of the filter, respectively.

Then, giving rise to the resources, the Binary Standards are computed for the magnitude and phase components of the filtered images. They are obtained when calculated using the DM, yielding Local Depth Gabor Binary Patterns (LDGBP). This new descriptor is obtained by multiplying Eq. (14) by the Fourier transform for images of the DM into four different scales and four orientations, and then the inverse transform is made to find the resulting Gabor coefficient described by the equation as follows:[2]

$$g(x,y) = F^{-1}(GF(I)) \tag{15}$$

where I is the image, F is the Fourier transform in 2D, and G is the Gabor radial filter multiplied by the angular Gaussian component.

The magnitude and phase of this descriptor are then taken as new images $g_M(x, y) = |g(x, y)|$ and $< g(x, y)$. The Binary Pattern algorithm is then applied to each of the resulting images to encode the structural information and also encode the phase information in each image using a variant of the LBP method because of the circular nature of the phase. In this case, a difference is made between the phase at the center point and at the two neighboring points, and this difference is compared to a threshold value Ψ so as to assign a value of zero or one for each neighbor point. For this case, the limit value was defined as $\pi/4$. Therefore, the LDGBP operator applied to the Gabor depth characteristic phase is calculated as:[2]

$$LDGBP(xc,yc) = \sum_{P=0}^{P-1} 2^P s(\Psi - |gp(xc,yc) - gp(xp,yp)|) \tag{16}$$

where $gp(xc, yc)$ is the image of the phase at the center point and $gp(xp, yp)$ is the phase image at the Pth point in the neighborhood of the point P, where P is the number of points in the neighborhood.[2]

Examples of magnitude and phase LDGBP images are shown in Figs. 6(c) and 6(d), respectively. All examples images were implemented through laboratory programs and are similar to those presented in Refs. 2, 16, 38 and 40 which suggests that the resources were correctly implemented, providing further confirmation of the method used.

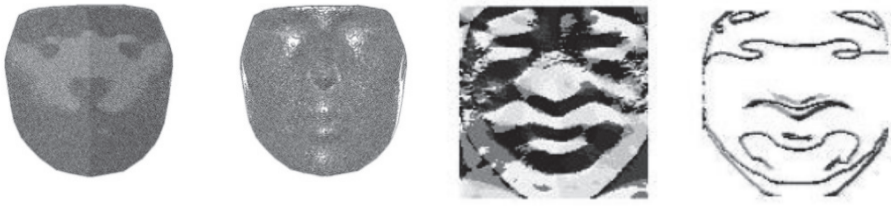

(a) (b) (c) (d)

Fig. 6. (a) LDPQ, (b) LAPQ, (c) LDGBPm and (d) LDGBPp for a subject in the database.[37]

6. Tests

As already mentioned, firstly a new database was created with DM, APDI, 3DLBP, LABP, LDPQ, LAPQ, LDGBPm and LDGBPp images from the 4D dataset.[37]

The following tests fix the T_{af} to 80%, and each expression is used to generate the detector set in the censor phase. It is emphasized that the censor phase uses only one expression to generate the dataset, and in the monitoring phase, every expression is used to realize the classification. The percentage of right and incorrect detection, mean values and pattern deviation (Tables 1 and 3) and censor and monitoring times (Tables 2 and 4) are presented.

The following equation is used to determine the pattern deviation:

$$S = \sqrt{\frac{1}{n-1}\sum_{i=1}^{n}(x_i - \bar{x})^2} \tag{17}$$

where n is the quantity of elements, x_i is the value corresponding to element i and $\bar{x}$ is the arithmetic mean.

The next section presents all of the test results.

7. Results of the AIS

This section presents the results obtained by applying the proposed methodology to the facial image dataset.[37] The AIS was developed in MATLAB®,[46] with the main objective being evaluation of the best descriptor and the best expressions to accomplish IR.

Table 1 presents Correct Detection (CD) and Incorrect Detection (ID) percentages for DM, APDI, 3DLBP, and LABP images.

Int. J. Artif. Intell. Tools 2019.28. Downloaded from www.worldscientific.com
by 14.145.175.103 on 03/18/20. Re-use and distribution is strictly not permitted, except for Open Access articles.

Int. J. Artif. Intell. Tools 2019.28. Downloaded from www.worldscientific.com
by 14.145.175.103 on 03/18/20. Re-use and distribution is strictly not permitted, except for Open Access articles.

Table 1. IR results for the DM, APDI, 3DLBP and LABP images calculated from the images in the database.[37]

	DM		APDI		3DLBP		LABP	
Expression	CD	ID	CD	ID	CD	ID	CD	ID
Angry	90.77	9.23	98.81	1.19	98.21	1.79	92.86	7.14
Contempt	91.37	8.63	98.81	1.19	97.02	2.98	95.54	4.46
Disgust	**91.96**	8.04	**99.40**	0.60	95.54	4.46	90.18	9.82
Fear	90.77	9.23	99.11	0.89	**99.11**	0.89	95.54	4.46
Happy	87.50	12.50	97.92	2.08	94.64	5.36	94.64	5.36
Phrase	88.39	11.61	97.92	2.08	96.13	3.87	91.96	8.04
Sad	89.29	10.71	**99.40**	0.60	99.10	0.90	**95.83**	4.17
Surprise	89.88	10.12	97.62	2.38	98.51	1.49	94.64	5.36
Mean	89.99	10.01	98.62	1.38	97.28	2.72	93.90	6.10
Pattern Deviation	±1.52	±1.52	±0.71	±0.71	±1.71	±1.71	±2.03	±2.03

The results from the images generated from the 2D facial geometry, called DM, present good IR results. The expression disgust presents the maximum classification index and the expression happy the minimum, being 91.96% and 87.5%, respectively. In general, every expression has good performance, with a mean of 89.99% ±1.52. The results using images generated from the 2D facial geometry, APDI, present the expressions disgust and sad when used as detectors; they performed at approximately 99.40%, which is an excellent index. The expression surprise gave the lowest correct classification, but it was still excellent at 97.62%. The performance mean is 98.62±0.71, which is a better result than that obtained from using the DM.

For the tests using images generated from the Binary Pattern characteristics called LBP and using the DM representation to originate the 3DLBP, the expression fear has the best performance of 99.11% when used as a detector. Therefore, the 3DLBP demonstrates good performance with a mean of 97.28% ± 1.71. Still based on the LBP and the APDI representation, the LABP is originated. The expression sad, when used as a detector, presents the best index, classifying 95.83% as right. Using the disgust images as censors, the lowest classification index was obtained, with 90.18%. The IR based on the LABP presents a right classification mean of 93.90% ± 2.03.

As noted by Sandbach *et al.*,[2] DM-based features provide more accurate results than those computed for APDI, and this observation becomes clear based on these two tests because the mean right classification for 3DLBP (a resource based on DM) was 97.28% ± 1.71 against the correct classification mean for LABP (a resource based on APDI) of 93.90% ± 2.03. It is noteworthy that most of the current papers do not present results of individual identity recognition independent of facial expression as is done in this paper. For example, Sandback *et al.*,[2] and *Moeslund et al.*[3] are based on the detection and classification of AUs, and it is necessary to use additional methods (histogram or Multi-Scale Extended) to detect and classify AU. Huang *et al.*[38] presents IR results only for Neutral expression and also makes use of a preprocessing step using cubic interpolation technique. A recent approach described by Lu *et al.*[47] uses LBP based on heat kernel volume to generate new descriptors of multiple orientation plans to then perform IR. These

additional methods required for these cases lead to a greater computational effort and a longer processing time to obtain the results. In Soyel and Demirel,[44] Kollias and Zafeiriou[48] and Jiang and Su[49] an ANN-based method with excellent performance for several facial expressions was approached, and still in Alvarez *et al*.[50] was implemented a classifier based on an ANN and logic fuzzy. However, this technique requires the images to undergo an initial process of vectoring the images to perform the training of the Neural Network, which procedure may take hours or days depending on the vector data and the size of the database. After ANN training, the response is considerably quick (seconds), however, this type of system is, in practical terms, inapplicable.

Table 2 presents the Censor Times (CT) and Monitoring Times (MT), in seconds, for the DM, APDI, 3DLBP and LABP images.

Table 2. Censor and monitoring times for the DM, APDI, 3DLBP and LABP images.

	DM		APDI		3DLBP		LABP	
Expression	CT	MT	CT	MT	CT	MT	CT	MT
Angry	44.07	118.4	44.21	117.4	41.74	111.2	50.07	115.6
Contempt	44.34	119.2	50.43	119.2	42.17	109.6	46.27	113.1
Disgust	43.95	118.8	47.67	115.2	42.73	107.4	45.06	113.2
Fear	42.59	118.6	45.82	123.2	41.57	109.2	45.97	111.5
Happy	42.85	117.8	44.63	113.9	42.92	111.0	45.65	111.4
Phrase	42.63	120.8	46.16	111.8	42.98	113.5	45.39	112.6
Sad	44.64	121.0	46.39	115.8	42.29	108.8	46.03	115.4
Surprise	45.54	121.2	45.76	116.9	42.13	112.8	45.50	115.2
Mean	43.83	119.5	46.38	116.7	42.32	110.4	46.24	113.5
Pattern Deviation	±1.06	±1.34	±1.95	±3.46	±0.52	±2.08	±1.59	±1.70

It is easily observed that the censor and monitoring times do not directly influence the classification of the images and that they have extremely approximate values and low pattern deviation. This shows that in addition to excellent IR correct detection rates, the complete runtime has decreased by approximately 190 seconds for the censor time and approximately 600 seconds for the monitoring time compared to what was presented by Silva *et al.*[19] In addition, no SIA-based reference was found for identity recognition that shows the processing time of the proposed system. This is an excellent decrease in the time of execution, encouraging the advancement of this research and the implementation of AIS in conjunction with the IR techniques presented in the methodology of this work.

Table 3 presents correct and incorrect detection percentages for LDPQ, LAPQ, LDGBPm and LDGBPp images. In the next tests, we will use images obtained from the descriptors based on the LPQ and GBP methods. The LPQ method extracts local phase information that contains important directional features that describe facial deformations (Fourier phase spectrum), and with the GBP method, it is possible to improve the facial features, improving the robustness of the LBP when there are changes of illumination, and the descriptors of this method are still possessed of a component of magnitude and a component of phase.

Int. J. Artif. Intell. Tools 2019.28. Downloaded from www.worldscientific.com
by 14.145.175.103 on 03/18/20. Re-use and distribution is strictly not permitted, except for Open Access articles.

Int. J. Artif. Intell. Tools 2019.28. Downloaded from www.worldscientific.com
by 14.145.175.103 on 03/18/20. Re-use and distribution is strictly not permitted, except for Open Access articles.

Table 3. IR results for the LDPQ, LAPQ, LDGBPm and LDGBPp images calculated from the images in the database.[37]

	LDPQ		LAPQ		LDGBPm		LDGBPp	
Expression	CD	ID	CD	ID	CD	ID	CD	ID
Angry	49.65	50.35	2.12	97.88	98.51	1.49	95.54	4.46
Contempt	4861	51.39	2.08	97.92	97.32	2.68	96.13	3.87
Disgust	47.31	52.69	2.16	97.84	99.40	0.60	95.83	4.14
Fear	45.14	54.86	**8.33**	91.67	**99.70**	0.30	97.32	2.68
Happy	**63.54**	36.46	2.68	97.32	98.51	1.49	96.73	3.27
Phrase	47.92	52.08	4.17	95.83	98.21	1.79	94.64	5.36
Sad	47.57	52.43	3.87	96.13	99.11	0.89	**97.62**	2.38
Surprise	42.01	57.99	2.21	97.79	97.32	2.68	94.94	5.06
Mean	48.97	51.03	3.45	96.55	98.51	1.49	96.09	3.90
Pattern Deviation	±6.34	±6.34	±2.14	±2.14	±0.89	±0.89	±1.07	±1.07

The LPQ method computed for the facial geometric representation DM gives the descriptor named LDPQ and did not exhibit good performance together with the recognition technique proposed in this work. The expression that obtained the best index of correct detection classification was happy, with 63.54%. Compared with previous results, this expression obtained results of up to 94.64% for the 3DLBP descriptor, which is also based on DM. The expression that obtained the lowest classification performance was surprise with 42.01% accuracy, and compared to previous tests based on DM, this same expression obtained an index of up to 98.51% (also for the 3DLBP descriptor). It is concluded that this descriptor does not perform well in conjunction with the AIS-based recognition technology strategy, obtaining an average rating of 48.97% ± 6.34.

The low rate of correct detections can also be observed for the tests using images based on the LPQ applied to the APDI that gave rise to the LAPQ descriptor. The expression that obtained the best index of correct classification was fear with 8.33%, showing itself to be an inefficient descriptor compared to the results obtained from other descriptors: 99.11% for the geometric representation APDI and 95.54% for the descriptor LABP (LBP applied to APDI). The expression that obtained the lowest classification performance was contempt with 2.08% correct detections. Compared with previous tests based on APDI, this same expression obtained an index of up to 95.54% (also for the LABP descriptor). It is also worth noting the observation made by Sandbach *et al.*[2] that DM-based resources provide more accurate results than those computed for APDI, and in fact, this can be observed even with the unsatisfactory results obtained for the LPQ method. Finally, it is concluded that the LABP descriptor does not perform well in conjunction with the AIS-based recognition technology strategy, obtaining a low classification average of only 3.45% ± 2.14.

For the last two tests, images generated from the descriptors based on the method of Gabor Filters that were computed using the DM giving rise to LDGBPm and LDGBPp will be used. For the tests based on the GBP method, no images were computed using the APDI, since as noted by Sandbach *et al.*[2] and in the previous tests of this work, DM-based features provide more accurate results than those computed for APDI.

Int. J. Artif. Intell. Tools 2019.28. Downloaded from www.worldscientific.com
by 14.145.175.103 on 03/18/20. Re-use and distribution is strictly not permitted, except for Open Access articles.

For the images from the LDGBP descriptor based on the magnitude component (LDGBPm), the expression with the best performance was the expression fear, presenting an excellent correct classification index of 99.70%. The expressions that obtained the lowest indexes, but still satisfactory indexes, were contempt and surprise, both with 97.32%. It is concluded that this is an excellent technique for IR when combined with the AIS-based recognition technology. With an average classification of 98.51% ± 0.89, it becomes the descriptor applied to the DM with the best results. Finally, images from the LDGBP descriptor based on the phase component (LDGBPp) were used. The expression with the best performance was the sad expression with an excellent classification index of correct detections of 97.62%, and the expression that obtained the lowest classification index was phrase with 94.64%. It can be concluded that the IR from the GBP method computed for the DM based on the phase component obtained a good performance with a mean of 96.09% ± 1.07. Even with good results, it is worth noting that this same technique, when computed for the magnitude component, obtained slightly better results.

Compared with existing approaches it can be seen that the GBP based descriptors provide the best results with the non-statistic based face representation approach in which the generalization problem is naturally avoided. In Zhang *et al.*[16] a promising GBP-based approach is proposed in which the authors make use of additional methods where the face image is modeled as a histogram sequence by concatenating the histograms of all the local regions of all the local Gabor magnitude binary pattern maps. Huang *et al.*[40] present a complementary method using global statistics as a good representation of geometric features for 3D facial recognition. Zhang *et al.*[44] need to use the Fisher separation criterion to improve the performance of the Gabor-based proposal. Ojansivu and Heikkilä[15] propose a new LPQ-based descriptor, but their facial texture recognition rates do not reflect the promising IR rates presented in this research. Musci *et al.*[42] presents a comparative analysis of LBP and LPQ techniques added to methods of extracting contrast information. Eleyan and Ashir[51] use a normalization algorithm for vector extraction, with promising comparative results of LPQ and GBP-based descriptor techniques. However, as previously noted, these additional methods required for these cases lead to a greater computational effort and a longer processing time to obtain the results, which entails a higher cost for practical applications of the mentioned methodologies.

Table 4 presents Censor and Monitoring times, in seconds, for the LDPQ, LAPQ, LDGBPm and LDGBPp images. Again, it can be observed that the censor and monitoring times do not influence the classification of the images and that they have extremely approximate values and low pattern deviation.

Even for the LAPQ descriptor that had the worst rates of correct detection, the censor and monitoring time remained practically the same as the others. However, the total execution time is extremely minor compared to Silva *et al.*,[19] clearly showing that the implementations of IR techniques presented in this work are feasible and encouraging. Besides, as mentioned, no specialized reference in IR with AI was found showing the times of execution, which further enhances this research, providing an important and unprecedented contribution.

Int. J. Artif. Intell. Tools 2019.28. Downloaded from www.worldscientific.com
by 14.145.175.103 on 03/18/20. Re-use and distribution is strictly not permitted, except for Open Access articles.

Table 4. Censor and Monitoring times for LDPQ, LAPQ, LDGBPm and LDGBPp images.

	LDPQ		LAPQ		LDGBPm		LDGBPp	
Expression	CT	MT	CT	MT	CT	MT	CT	MT
Angry	49.06	109.42	45.43	121.46	43.96	110.18	42.62	113.20
Contempt	40.69	107.47	46.63	117.39	43.13	110.06	42.36	114.21
Disgust	41.98	108.67	47.50	118.10	43.80	111.46	43.16	114.44
Fear	49.73	108.21	47.13	120.75	42.61	112.53	43.97	112.76
Happy	40.12	109.46	46.48	118.30	42.94	108.36	42.36	113.93
Phrase	49.65	108.02	47.32	118.59	44.91	108.69	43.62	112.23
Sad	40.06	108.64	47.00	117.52	42.55	109.92	42.71	112.82
Surprise	49.64	109.30	51.54	126.05	44.41	111.12	42.77	113.31
Mean	45.12	108.65	47.38	119.77	43.54	110.29	42.95	113.36
Pattern Deviation	±4.75	±0.72	±1.80	±2.94	±0.87	±1.39	±0.63	±0.77

Based on the results obtained with the AIS, it is possible to conclude it to be robust and precise and to confer security and reliability for IR. Furthermore, it is emphasized that the best performance of the NSA on the tests efficiently realized the proposal aims. These results drive the need for continued proposals in this area.

Considering the theoretical research, eight different facial expressions images were used for the Censor phase of the AIS aiming to evaluate which is the best expression to perform the IR.

In addition, several techniques of information analysis of the 3D facial geometry proposed as functionalities for Binary Pattern and denominated as descriptors were approached. Through the results and bibliographies used for the development of the proposed methodology, it was evident that the techniques that provide the best results for the recognition of pattern in images, using the system based on the technological strategy of the AIS for IR, were APDI and GBP. In this way, it is concluded that the applicability of the methodology based on these two descriptors, validated with the performance of the new IR solution based on SIA, will be promising.

8. Conclusion and Suggestions for Future Work

This paper presents an IR method based on facial biometry realized with the NSA based on the AIS. The images used were generated from binary characteristic representations (DM and APDI) with the most used 2D facial geometries (LBP, LPQ and GBP). Eight new facial descriptors were developed, and a new database was created. The AIS is used with this new database to realize the IR and validate the proposed method.

The best performance is the APDI descriptor, recognizing approximately 98.62% ± 0.71. The LDGBPm follows with 98.51%±0.89, the 3DLBP follows with 97.28% ± 1.71, and then the LDGBPp with 96.09%±1.07. The expression used as the detector with the best correct classification index is fear from the LDGBPm descriptor with 99.70%, followed by the expression disgust (to LDGBPm), disgust and sad (to APDI) with 99.40% and the expression sad (to LDGBPm) and fear (to APDI and 3DLBP), both

with 99.11%. Based on the results obtained, it is concluded that the system based on the AIS technology strategy for the accomplishment of the IR presented robustness, precision, safety and reliability. In addition, it is worth mentioning the excellent performance that the NSA presented in performing the tests performed, making it possible to achieve the objectives proposed in this work and revealing its efficiency and effectiveness.

The approach used in this paper is just one of many possible ways to apply AIS. Considering the satisfactory results obtained in the execution of the tests, some suggestions for the exploration of this study can be highlighted, such as incorporation of other AIS strategies, as for example, the Dendritic Cell Algorithm; application of disturbances to images of the monitoring phase to evaluate its ability to classify; use of other software for possible decreases in censor and monitoring time, thus reducing the computational effort; and application of this technological alternative of AIS-based IR in routine processes, such as a security system in ATM transactions in which the individual inserts the card into the machine and a camera captures an image of the person and performs the recognition, identifying if he is actually the owner of the card. Furthermore, as a futuristic prospect, it can be said that the use of magnetic cards will be outdated and that there will be no need to insert cards in the machine because, by facial biometry, the ATM will recognize the person and release the transactions. There are so many other possible applications not limited to engineering but expanding studies to provide well-being of people, the fundamental role of the scientific community.

Acknowledgment

The authors thank CAPES (Coordenação de Aperfeiçoamento de Pessoal de Nível Superior, Brazil), CAPES/PDSE (Process: BEX 18730-12-4, Brazil), and ISR — Institute of Systems and Robotics — University of Coimbra, Portugal.

References

1. M. Nicolaou, H. H. Gunes and M. Pantic, Continuous prediction spontaneous affect from multiple cues a modalities valence-arousal space, *IEEE Transactions on Affective Computing* **2**(2) (June 2011) 92–105.
2. G. Sandbach, S. Zafeiriou and M. Pantic, Binary pattern analysis for 3d facial action unit detection, in *Proc. of the British Machine Vision Conf.* (*BMVC' 12*) (Canada, 2012), pp. 119.1–119.12.
3. T. B. Moeslund, A. Hilton, V. Krüger and L. Sigal (eds.), *Facial Expression Analysis. Visual Analysis of Humans: Looking at People*, 1st edn. (Springer-Verlag, New York, 2011).
4. X. Li, Q. Ruan and Y. Ming, 3D facial expression recognition based on basic geometric features, *IEEE Int. Conf. on Signal Processing* (*ICSP 2010*) (October 24–28, 2010), pp. 1366–1369.
5. T. Sha, M. Song, J. Bu, C. Chen and D. Tao, Feature level analysis for 3D facial expression recognition, *Neurocomputing* **74**(12–13) (June 2011) 2135–2141.
6. H. Soyel and H. Demirel, Optimal feature selection for 3D facial expression recognition using coarse-to-fine classification, *Turkish Journal of Electrical Engineering and Computer Sciences* **18**(6) (2010) 1031–1040.

Int. J. Artif. Intell. Tools 2019.28. Downloaded from www.worldscientific.com
by 14.145.175.103 on 03/18/20. Re-use and distribution is strictly not permitted, except for Open Access articles.

Int. J. Artif. Intell. Tools 2019.28. Downloaded from www.worldscientific.com
by 14.145.175.103 on 03/18/20. Re-use and distribution is strictly not permitted, except for Open Access articles.

7. P. Lemaire, B. B. Amor, M. Ardabilian, L. Chen and M. Daoudi, Fully automatic 3D facial expression recognition using a region-based approach, *in Proc. of the 2011 Joint ACM Workshop on Human Gesture and Behavior Understanding* (*J-HGBU*) (2011), pp. 53–58.
8. A. Maalej, B. B. Amor, M. Daoudi, A. Srivastava and S. Berretti, Shape analysis of local facial patches for 3D facial expression recognition, *Pattern Recognition* **44**(8) (August 2011)1581–1589.
9. I. Mpiperis, S. Malassiotis and M. Strintzis, Bilinear decomposition of 3D face images: An application to facial expression recognition, *10th Int. Workshop on Image Analysis for Multimedia Interactive Services* (*WIAMIS' 2009*) (May 6–8, 2009), pp. 1–4.
10. X. Zhao, E. D. Di Huang and L. Chen, Automatic 3D facial expression recognition based on a Bayesian belief net and a statistical facial feature model, *IEEE Int. Conf. on Pattern Recognition* (*ICPR 2010*) (August 23–26, 2010), pp. 3724–3727.
11. S. Berretti, B. B. Amor, M. Daoudi and A. D Bimbo, 3D facial expression recognition using SIFT descriptors of automatically detected keypoints, *The Visual Computer* **27**(11) (2011) 1021–1036.
12. T. Ojala, M. Pietikäinen and T. Mäenpää, Multiresolution gray-scale and rotation invariant texture classification with local binary patterns, *IEEE Transactions on Pattern Analysis and Machine Intelligence* **24**(7) (July 2002) 971–987.
13. C. Shan, S. Gong and P. W. McOwan, Facial expression recognition based on local binary patterns: A comprehensive study, *Image and Vision Computing* **27**(6) (May 2009) 803– 816.
14. T. Ahonen and A. Hadid, Face description with local binary patterns: Application to face recognition, *IEEE Transactions on Pattern Analysis and Machine Intelligence* **28**(12) (December 2006) 2037–2041.
15. V. Ojansivu and J. Heikkilä, Blur insensitive texture classification using local phase quantisers, *Int. Conf. on Image and Signal Processing* (*ICISP 2008*) (July 1–3, 2008), pp. 236–243.
16. W. Zhang, S. Shan, W. Gao, X. Chen and H. Zhang, Local Gabor binary pattern histogram sequence (LGBPHS): A novel non-statistical model for face representation and recognition, *IEEE Int. Conf. on Computer Vision* (*ICCV 2005*) (October 17–21, 2005), pp. 786–791.
17. A. Savran, B. Sankur and M. T. Bilge, Comparative evaluation of 3D vs. 2D modality for automatic detection of facial action units, *Pattern Recognition* **45**(2) (February 2012) 767–782.
18. B. J. Matuszewski, W. Quan, L-K. Shark, A. S. Mcloughlin, C. E. Lightbody, H. C. A Emsley and C. L. Watkins, HI4D-ADSIP 3-D dynamic facial articulation database, *Image and Vision Computing* **30**(10) (October 2012) 713–727.
19. J. C. Silva, F. P. A. Lima, A. D. P. Lotufo and J. M. Batista, Identity recognition using an artificial intelligence based on artificial immune system, *IEEE 3rd Asia-Pacific Conf. on Computer Aided System Engineering* (*APCASE 2015*) (July 14–16, 2015), pp. 158–162.
20. J. Wang, L. Yin, X. Wei and Y. Sun, 3D facial expression recognition based on primitive surface feature distribution, *IEEE Computer Society Conf. on Computer Vision and Pattern Recognition* (*CVPR 2006*) (June 17–22, 2006), pp. 1399–1406.
21. M. Rosato, X. Chen and L. Yin, Automatic registration of vertex correspondences for 3D facial expression analysis, *IEEE Int. Conf. on Biometrics: Theory, Applications and Systems* (*BTAS 2008*) (September 29–1 October, 2008), pp. 1–7.
22. O. Ocegueda, T. Fang, S. K. Shah and I. Kakadiaris, Expressive maps for 3D facial expression recognition, *IEEE Int. Conf. on Computer Vision Workshops* (*ICCV Workshops*) (November 6–13, 2011), pp. 1270–1275.
23. A. Maalej, B. B. Amor, M. Daoudi, A. Srivastava and S. Berretti, Local 3D shape analysis for facial expression recognition, *IEEE Int. Conf. on Pattern Recognition* (*ICPR 2010*) (August 23–26, 2010), pp. 4129–4132.

Int. J. Artif. Intell. Tools 2019.28. Downloaded from www.worldscientific.com
by 14.145.175.103 on 03/18/20. Re-use and distribution is strictly not permitted, except for Open Access articles.

24. S. Ramanathan, A. Kassim, Y. V. Venkatesh and W. S. Wah, Human facial expression recognition using a 3D morphable model, *IEEE Int. Conf. on Image Processing* (*ICIP 2006*) (October 8–11, 2006), pp. 661–664.
25. A. Savran and B. Sankur, Automatic detection of facial actions from 3D data, *IEEE Int. Conf. on Computer Vision Workshops* (*ICCV Workshops*) (September 27–October 1, 2008), pp. 1993–2000.
26. D. Chen and Y. Zhang, Robust zeroing neural-dynamics and its time-varying disturbances suppression model applied to mobile robot manipulators, *IEEE on Neural Networks and Learning Systems* **29**(9) (September 2018) 4385–4397.
27. D. Chen, Y. Zhang and S. Li, Tracking control of robot manipulators with unknown models: A Jacobian-matrix-adaption method, *IEEE Transactions on Industrial Informatics* **14**(7) (July 2018) 3044–3053.
28. D. Chen and Y. Zhang, A hybrid multi-objective scheme applied to redundant robot manipulators, *IEEE Transactions on Automation Science and Engineering* **14**(3) (July 2017) 1337–1350.
29. D. Chen, Y. Zhang and S. Li, Zeroing neural-dynamics approach and its robust and rapid solution for parallel robot manipulators against superposition of multiple disturbances, *Neurocomputing* **275** (January 2018) 845–858.
30. I. Mpiperis, S. Malassiotis and M. Strintzis, Bilinear elastically deformable models with application to 3D face and facial expression recognition, *IEEE Int. Conf. on Automatic Face & Gesture Recognition* (*FG 2008*) (September 17–19, 2008).
31. D. Dasgupta (ed.), *Artificial Immune Systems and Their Applications*, 1st edn. (Springer-Verlag, New York, 1998).
32. L. N. De Castro and J. Timmis, *Artificial Immune Systems: A New Computational Intelligence Approach*, 1st edn. (Springer, London, 2002).
33. S. Forrest, A. S. Perelson, L. Allen and R. Cherukuri, Self-nonself discrimination in a computer, *IEEE Computer Society Symp. on Research in Security and Privacy* (SP 1994) (May 16–18, 1994), pp. 202–212.
34. F. P. A. Lima, A. D. P. Lotufo and C. R. Minussi, Artificial immune systems applied to voltage disturbance diagnosis in distribution electrical systems, *IEEE PowerTech* (*POWERTECH 2013*) (June 16–20, 2013), pp. 1–6.
35. F. P. A. Lima, A. D. P. Lotufo and C. R. Minussi, Disturbance detection for optimal database storage in electrical distribution systems using artificial immune systems with negative selection, *Electric Power System Research* **109** (April 2014) 54–62.
36. D. W. Bradley and A. M. Tyrrell, Immunotronics-novel finite-state-machine architectures with built-in self-test using self-nonself differentiation, *IEEE Transactions on Evolutionary Computation* **6**(3) (June 2002) 227–238.
37. 4D facial database, identity recognition using 4D-facial dynamics (University of Coimbra, Institute of Systems and Robotics, 2012).
38. D. Huang, M. Ardabilian, Y. Wang and L. Chen, A novel geometric facial representation based on multi-scale extended local binary patterns, *IEEE Int. Conf. on Automatic Face & Gesture Recognition* (*FG 2011*) (March 21–25, 2011), pp. 1–7.
39. A. V. Oppenheim and J. S. Lim, The importance of phase in signals, in *Proc of the IEEE* **69**(5) (May 1981) 529–541.
40. Y. Huang, Y. Wang and T. Tan, Combining statistics of geometrical and correlative features for 3D face recognition, *British Machine Vision Conf.* (*BMVA 06*) (Edinburgh, 2011), pp. 879–888.
41. M. R. Banham and A. K. Katsaggelos, Digital image restoration, *IEEE Signal Processing Magazine* **14**(2) (March 1997) 24–41.

42. M. Musci, R. Q. Feitosa, M. L. Velloso, T. Novack and G. O. Costa, An evaluation of texture descriptors based on local binary patterns for classifications of remote sensing images, *Boletim de Ciencias Geodésicas* **17**(4) (October–December 2011) 549–570.
43. D. Gabor, Theory of communication, *Journal of the Institution of Eletrical Engineers – Part I: General* **94**(73) (1947) 429–457.
44. H. Soyel and H. Demirel, Facial expression recognition using 3D facial feature distances, *4th Int. Conf. Image Analysis and Recognition* (*ICIAR 2007*) (August 22–24, 2007), pp. 831–838, 2007.
45. B. Zhang, S. Shan, X. Chen and W. Gao, Histogram of Gabor phase patterns (HGPP): A novel object representation approach for face recognition, *IEEE Transactions on Image Processing* **16**(1) (January 2007) 57–68.
46. MATLAB 7.8 Version, Mathworks Company.
47. W. Lu, Xi. Yang, X. Gou, L. Jian, W. Wu and G. Jeon, Parallel heat kernel volume based local binary pattern on multi-orientation planes for face representation, *International Journal of Parallel Programming* **46** (5) (Octuber 2018) 943–962.
48. D. Kollias and S. Zafeiriou, Training deep neural networks with different datasets in-the-wild: The emotion recognition paradigm, *International Joint Conf. on Neural Networks* (*IJCNN*) (July 8–13) (Rio de Janeiro, 2018), Vol. 1809.04359.
49. C. Jiang and J. Su, Gabor binary layer in convolutional neural networks, *25th IEEE Int. Conf. on Image Processing* (*ICIP 2018*) (October 7–10) (Athens, Greece) pp. 3008–3412.
50. V. M. Alvarez, R. Velazquez, S. Gutierrez and J. Enriquez-Zarate, A method for facial emotion recognition based on interest points, *Int. Conf. on Research in Intelligent and Computing in Engineering* (RICE) (El Salvador, August 22–24, 2018).
51. A. Eleyan and A. M. Ashir, A monogenic local gabor binary pattern for facial expression recognition, *Selcuk University Journal of Engineering, Science and Technology* **5**(4) (December 2017) 414–422.

Int. J. Artif. Intell. Tools 2019.28. Downloaded from www.worldscientific.com
by 14.145.175.103 on 03/18/20. Re-use and distribution is strictly not permitted, except for Open Access articles.